








RESEARCH ARTICLE | FEBRUARY 29 2024

Point projection radiography of electromagnetically accelerated flyer plates with an external X-pinch driver

J. Read ; G. Burdiak ; S. N. Bland ; L. S. Caballero Bendixsen ; L. Paxton-Fear ; N. Niasse ; C. Dobranszki ; N. Hawker

 Check for updates

Rev. Sci. Instrum. 95, 023508 (2024)

<https://doi.org/10.1063/5.0185351>



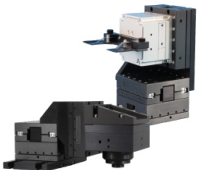
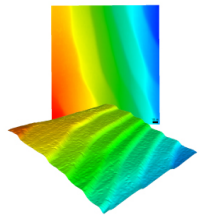
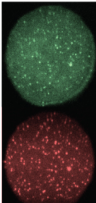


View
Online



Export
Citation

CrossMark

 <p>MCL MAD CITY LABS INC. www.madcitylabs.com</p>	<p>Nanopositioning Systems</p> 	<p>Modular Motion Control</p> 	<p>AFM and NSOM Instruments</p> 	<p>Single Molecule Microscopes</p> 
--	--	--	---	--

Point projection radiography of electromagnetically accelerated flyer plates with an external X-pinch driver

Cite as: Rev. Sci. Instrum. 95, 023508 (2024); doi: 10.1063/5.0185351

Submitted: 30 October 2023 • Accepted: 31 January 2024 •

Published Online: 29 February 2024 • Publisher Error Corrected: 04 March 2024



View Online



Export Citation



CrossMark

J. Read,^{1,a)} G. Burdiak,¹ S. N. Bland,² L. S. Caballero Bendixsen,¹ L. Paxton-Fear,¹ N. Niasse,¹
C. Dobranszki,¹ and N. Hawker¹

AFFILIATIONS

¹First Light Fusion, Yarnton, Oxfordshire OX5 1QU, United Kingdom

²The Blackett Laboratory, Imperial College, London SW7 2BW, United Kingdom

^{a)}Author to whom correspondence should be addressed: joshua.read@firstlightfusion.com

ABSTRACT

A platform for flyer plate benchmarking experiments has been developed, with an external X-pinch driver for point projection radiography. The experiments were performed using CEPAGE, a low inductance pulsed power machine at First Light Fusion (2 MA, 1.4 μ s), with a new vacuum transmission line and flyer load hardware designed specifically to give a line of sight for radiography. A broadband 10–20 keV x-ray source was produced by a portable X-pinch driver (140 kA, 350 ns) [Strucka *et al.*, Matter Radiat. Extremes 7, 016901 (2021)] and was used to image the flyer. Radiography compliments the pre-existing diagnostic suite, which consists of current probes, velocimetry, and side-on optical probing of the impact shock transmitted into a transparent sample. The platform allows for significant insights into the 2D and 3D nature of the flyer launch, such as deformation and instability formation. It was used to diagnose a $10 \times 9 \times 1$ mm³ aluminum flyer, which reached a peak velocity of 4.2 km s⁻¹ before impact with a poly(methylmethacrylate) sample. The experimental configuration, on-shot source characterization, and the results from two flyer plate experiments on CEPAGE are discussed.

© 2024 Author(s). All article content, except where otherwise noted, is licensed under a Creative Commons Attribution (CC BY) license (<http://creativecommons.org/licenses/by/4.0/>). <https://doi.org/10.1063/5.0185351>

I. INTRODUCTION

Flyer plates are a type of electromagnetically launched projectile commonly used to drive shock Hugoniot and release equation of state (EoS) experiments on pulsed power facilities, such as Sandia's Z Machine.¹ Large currents are discharged through two parallel electrodes, which are separated by a small gap and connected at one end to form a short circuit. The opposing current directions in the electrodes produce a strong magnetic field in the anode–cathode (A–K) gap. The resultant $\vec{J} \times \vec{B}$ force accelerates the electrodes outward. Similar electrode configurations can be used to perform quasi-isentropic, ramp compression experiments.^{2,3}

For direct impact shock Hugoniot experiments, there is a requirement for the flyer plate front surface to remain solid on impact with a sample such that the impacted state can be determined to high accuracy.³ On the M3 pulsed power machine

(8.1 MA, 1.2 MJ, 1.8 μ s for flyer plate loads) at First Light Fusion (FLF), flyer plates are used to drive hydrodynamic pressure amplifiers.⁴ In this application, there is no requirement for a solid projectile, and the flyer plate is driven through the melt transition before impact, increasing the pulse length and peak pressure.

Flyer plates are typically diagnosed by measuring their front surface velocity using phase Doppler velocimetry (PDV) or velocity interferometry for any reflector (VISAR) and then drive current some distance from the load, which are compared to simulations. On M3, the VISAR signal is eventually lost during flyer plate launch due to several effects: a drop in reflectivity when the front surface vaporizes, distortion or tilt of the reflecting surface, and production of low density plasma obscuring the line of sight. As most flyer loads are made by recessing a thick (~10 mm) electrode to provide a thin plate that is easy to accelerate, the loss of velocimetry signal means the flyer remains undiagnosed until it exits the recess (see Fig. 1).

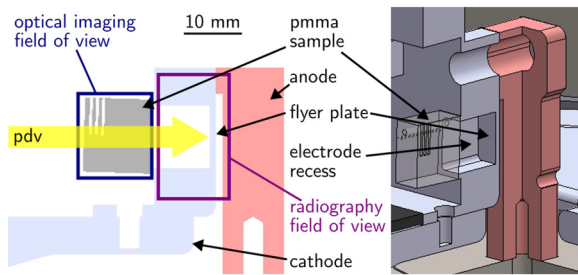


FIG. 1. The vertical load showing flyer plate features and the diagnostic lines of sight. During an experiment, the flyer plate accelerates toward the PMMA sample due to strong magnetic pressure in the A–K gap.

FLF uses B2, an in-house 3D multi-material radiative resistive magneto-hydrodynamics code, to model the coupled flyer and amplifier system. Previous experiments at FLF have used the temporal and spatial profile of a shock driven by the flyer into a transparent sample to constrain the simulations. This is useful for designing amplifiers as the shock pressure upon impact is critical information for optimizing the amplifier performance. Nevertheless, it is an integrated measurement, and more information is required to improve the predictive capabilities of the code.

Radiography provides an opportunity to obtain additional data on the flyer while it accelerates in the recess by probing through the electrode material before the flyer impacts the sample. X-pinchs are a pulsed-power-driven x-ray source that have previously been used for point projection radiography of high energy density physics (HEDP) experiments, usually by locating the load in the current return post of the main experiment.^{5–7} The current flows through two or more crossed wires, which ablate due to Ohmic heating before they are compressed by the $\vec{j} \times \vec{B}$ force at the crossing point, producing an intense μm -scale source of thermal x rays known as the hot-spot, predominantly with photon energies of several keV. This source is ideal for imaging biological samples,⁸ wire ablation flow experiments,^{9–11} and exploding wire cores.¹² Subsequent breakup of this hot spot leads to a larger ($>100 \mu\text{m}$) non-thermal source of higher energy photons, which may extend up to a significant fraction of the generator voltage.⁸

In this work, an external X-pinch driver was used to radiograph flyer plate experiments on a second pulsed power machine. The use of an external X-pinch driver affords more flexibility in timing and positioning the source compared to an X-pinch on the current return of the main experiment. Dry Pinch I is a portable ($30 \times 30 \times 70 \text{ cm}^3$) X-pinch driver developed at Imperial College London, designed to be resistant to electromagnetic interference. The source produced by $4 \times 30 \mu\text{m}^2$ Ag wires has previously been studied, and measurements of the source spectrum and size in different spectral bands have been published.¹³ Offline tests have shown a good contrast while radiographing a static flyer plate load at relevant distances.¹³

The addition of radiography to the diagnostic suite demonstrates the utility of Dry Pinch I as an external x-ray source for imaging HED experiments and provides additional data to compare with flyer plate simulations. The apparent areal density, flyer

deformation and tilt, electrode gap width, trailing mass, and instabilities can be observed in the radiography data.

II. EXPERIMENTAL SETUP AND DESIGN OF RADIOGRAPHY LINE OF SIGHT

Flyer plate experiments were performed on CEPAGE,¹⁴ a direct capacitor discharge, low inductance, pulsed power machine. It is well suited to rapid development work due to its small size (2 m diameter) and lower stored energy ($\sim 100 \text{ kJ}$), which results in less destructive shots compared to those performed on M3. In its original configuration, the power feed and flyer plate lie in the same plane as the transmission lines to minimize inductance. This load geometry precludes a view of the recessed electrode and A–K gap along the line of sight orthogonal to the flyer direction of travel. Similar load configurations are found on, for example, Veloce,¹⁵ THOR,² and Mach.¹⁶ An alternative load geometry, which is commonly employed on Sandia's Z machine, creates an accessible line of sight by orienting and raising the flyer out of the plane of the transmission line.¹⁷ Figure 1 shows this electrode geometry designed for CEPAGE. The flyer is 1 mm thick, 10 mm tall, and 9 mm wide (into the page).

A vacuum transition and transmission line were designed for CEPAGE to facilitate the new flyer plate design, which requires vacuum insulation instead of multi-layer plastic between the electrodes. These modifications, shown in Fig. 2, were based on the Shiva Star design;¹⁸ the details will form the subject of a future publication. The transmission line has a double helix structure with a sinusoidal surface profile to block any direct line of sight between the load region and the plastic vacuum diode, which was installed at the vacuum transition. The modifications increase the machine inductance, which increases the rise time from 600 ns to 1.4 μs .

The relative positioning of the source, object, and detector along the radiography line of sight is a trade-off between image intensity and resolution. The X-pinch emission is isotropic so the image intensity I follows an inverse square law,

$$I \propto (d_1 + d_2)^{-2}, \quad (1)$$

where d_1 is the source–object distance and d_2 is the object–detector distance. The resolution in the object plane δ_{obj} describes the apparent spatial extent of a sharp edge in the radiograph. It is related to the resolution at the image plane (detector location), δ_{img} by the point projection magnification, M ,

$$\delta_{obj} = \frac{\delta_{img}}{M} = \left(\frac{d_1 + d_2}{d_1} \right)^{-1} \cdot \sqrt{\delta_{det}^2 + \delta_{source}^2 + \delta_{edge}^2}. \quad (2)$$

The resolution at the detector is the quadrature sum of contributions from the detector resolution δ_{det} , source size δ_{source} , and the edge depth along the radiography line of sight δ_{edge} . The source and edge depth limited resolution can be obtained through geometric arguments, resulting in

$$\delta_{source} = \frac{d_2}{d_1} s, \quad (3)$$

$$\delta_{edge} = r_{edge} (d_1 + d_2) \frac{t_{edge}}{d_1^2}, \quad (4)$$

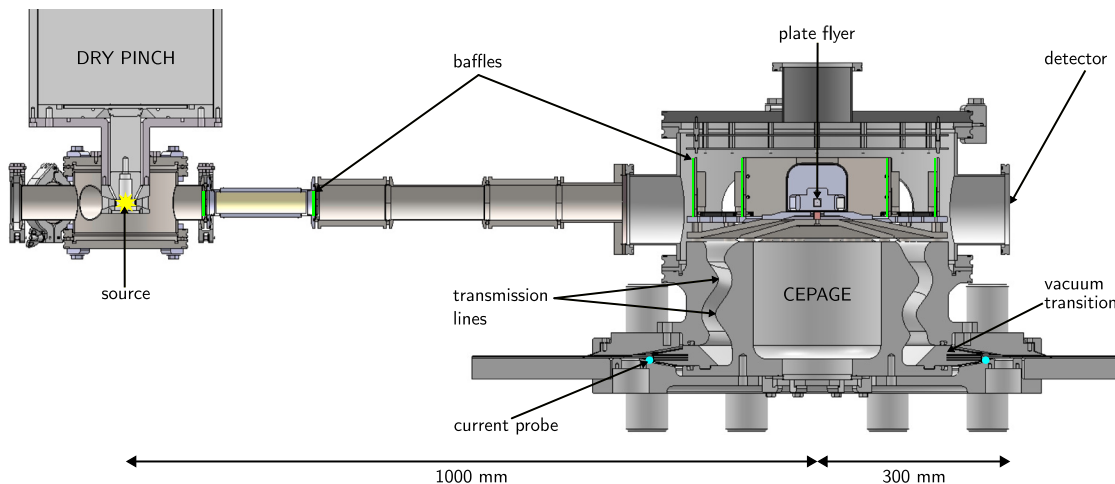


FIG. 2. Schematic of Dry Pinch I and CEPAGE coupling, showing the relative positions of the x-ray source, object, and detector. The vacuum transition and transmission lines that enable the vertical flyer plate load are labeled on CEPAGE. The baffles that block the debris are highlighted in green. Baffles in the CEPAGE chamber have polycarbonate windows over their apertures. Machine current was measured from Faraday rotation of light in a fiber loop indicated by the blue dots.

where s is source size, r_{edge} is the orthogonal distance from the imaging axis to the edge, and t_{edge} is the thickness of the edge along the line of sight.

Equation (2) was used to explore the design space for the radiography line to find the resolution dependence on d_1 and d_2 . The detector resolution was measured as $\delta_{det} = 115 \mu\text{m}$ by radiographing a sharp edge in contact with the detector (image plate) and by measuring the width between the 10%–90% signal levels. The edge depth limited resolution is calculated for a flyer plate midway along the electrode recess, which has a depth $t_{edge} = 9 \text{ mm}$ and a distance $r_{edge} = 15 \text{ mm}$ from the imaging axis. Un-like detector resolution, the edge depth limited resolution is sensitive to the relative positioning of the source, object, and detector. For distances $d_1 = 1000 \text{ mm}$ and $d_2 = 300 \text{ mm}$, the edge depth limited resolution is $\delta_{edge} = 176 \mu\text{m}$. Strucka *et al.* reported a source size of $190(100) \mu\text{m}$ measured from the width of a sharp edge through a $12.5 \mu\text{m}$ Ti filter onto the image

plate. The transmission and response data for this measurement are shown in Fig. 3 in blue. The $12.5 \mu\text{m}$ Ti filter has a 2.5–5 keV transmission window, which allows hot-spot radiation to pass. For our application, the x rays must penetrate the electrode recess walls, significantly attenuating the signal from the hot spot. In the present work, the source size was measured at 1.5 mm using a time integrated pinhole camera with a $200 \mu\text{m}$ Al filter. This filter does not have a low energy transmission window (orange data shown in Fig. 3) and is, therefore, a more appropriate measurement of source size for flyer plate experiments.

05 March 2024 09:30:57

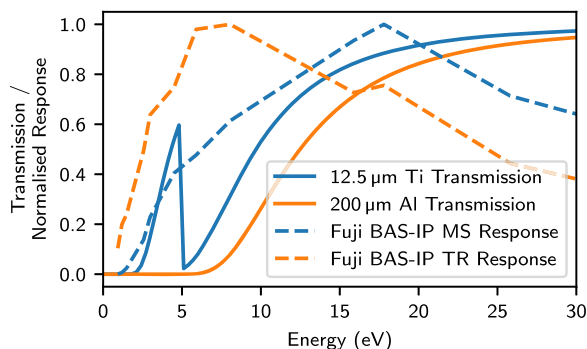


FIG. 3. Filter transmission curves (solid lines) and normalized image plate responses (dashed lines) used to make source size measurements for the resolution model. Data are taken from the experiments and modeling by Henke *et al.*¹⁹ and Meadowcroft *et al.*²⁰

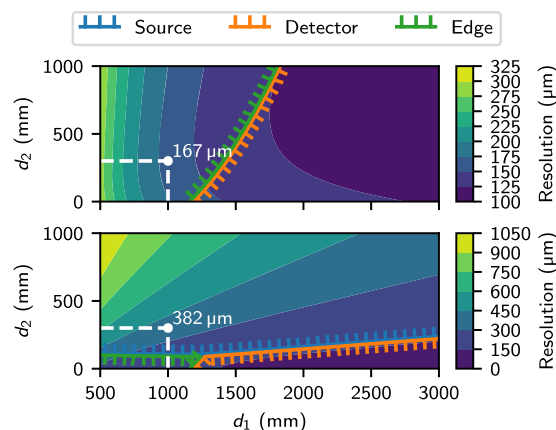


FIG. 4. Contour plot of the resolution model [Eq. (2)] over a range of source, object, and detector distances for source sizes of $190 \mu\text{m}$ (top) and 1.5 mm (bottom). The dominant source of spatial uncertainty for each region of the parameter space is indicated by the ticked contours. The distances used in the final radiography line of sight are indicated by the white dashed lines, and the white number is the system resolution at this point in the design space.

The top pane of Fig. 4 shows Eq. (2) evaluated for a source size of $190\ \mu\text{m}$. Depending on the choice of d_1 and d_2 , the resolution is either limited by the width of the flyer along the line of sight or the detector. The lower pane of Fig. 4 shows Eq. (2) evaluated for a source size of $1.5\ \text{mm}$. In this case, the source size dominates and the resolution is optimized by increasing d_1 and decreasing d_2 . In the final design, d_1 was set at $1000\ \text{mm}$, balancing the resolution with intensity, and d_2 was set at $300\ \text{mm}$ to provide sufficient stand off and ballistic shielding from the destructive flyer plate load. The resulting system has a magnification of $1.3\times$ and a theoretical resolution of $382\ \mu\text{m}$, which is acceptable for a cm scale flyer plate.

Dry Pinch I was connected to CEPAGE by a vacuum pipe as shown in Fig. 2. Its distance from CEPAGE can be adjusted, allowing the source to object distance to be tuned in the future experiments. The top transmission line and vacuum chamber of CEPAGE go to the capacitor voltage ($60\ \text{kV}$) during discharge of the machine. Consequently, the mounting hardware was made from a thick ($30\ \text{mm}$) acetal to electrically isolate the grounded casing of Dry Pinch I from CEPAGE. The vacuum systems of Dry Pinch I and CEPAGE were coupled together to avoid x-ray attenuation in thick window materials. A $200\ \text{mm}$ long ceramic vacuum pipe was used to maintain electrical isolation between CEPAGE and Dry Pinch I.

Baffles were placed along the radiography line of sight from the source to the detector to protect both the chambers from debris. Polycarbonate windows were placed across the clear aperture of the baffles to provide additional shielding. A total of $4\ \text{mm}$ of polycarbonate was present along the radiography line of sight, limiting the transmission of soft x rays (10% transmission cutoff energy equal to $8.4\ \text{keV}$). The field of view included the electrode gap, flyer plate, and the full height of the recess in the electrode. In the region ahead of the flyer, the combined $1\ \text{mm}$ depth of Al that forms the recess walls with the polycarbonate shielding results in a 10% transmission cutoff energy of $15.3\ \text{keV}$.

A time integrating image plate (FujiFilm BAS-TR) was used to detect the x rays due to the availability of inexpensive, large format sheets. The x-ray emission is gated by the X-pinch pulse width of $15\ \text{ns}$ (FWHM), resulting in a motion blur of $\sim 60\ \mu\text{m}$ for projectile traveling at $4\ \text{km}\ \text{s}^{-1}$. Dry Pinch I was triggered at different times relative to the CEPAGE discharge in order to capture the flyer at different positions in its trajectory.

Faraday rotation was used to measure the machine current through the area enclosed by a fiber loop, located by the plastic diode (blue dots in Fig. 2). A one-point PDV probe was used to measure the velocity at the center of the flyer front, and backlit optical imaging was used to measure the velocity of the shock imparted by the flyer in a poly(methylmethacrylate) (PMMA) sample (see Fig. 1).

III. SOURCE CHARACTERIZATION

X-pinch produces a structured, multi-component, and spectrally broadband source, which can vary from shot to shot. Understanding the source characteristics is required to accurately interpret the radiography images. The resolution depends on the source size, apparent areal density depends on the source spectrum, and motion blur depends on the pulse width. There is an un-obstructed line of sight about the azimuth of the X-pinch source, enabling on-shot

diagnostic access via independent lines of sight to characterize the source.

In the present work, two additional diagnostic lines of sight were fielded to provide on-shot source characterization. Direct image calibration was prioritized over detailed source characterization, which formed the subject of a previous publication.¹³ On one line, a combined grid and step-wedge target was used to measure the image resolution and calibrate areal density [Fig. 5(a)]. On the other line, filtered diodes were fielded to measure the x-ray pulse time and duration. In the future experiments, additional diagnostics may be fielded to make detailed simultaneous measurements of the source spectrum and structure.

The step wedge was machined into a single piece of aluminum arranged as a 3×3 grid, resulting in 9 discrete thicknesses ranging from 0.2 – $1.8\ \text{mm}$. Using the same material as the flyer means that flyer radiograph response can be directly referenced to the areal density from the step wedge. This simplifies analysis significantly under the assumption of cold opacity. Figure 5(b) shows the calibration curve from image plate response to aluminum step wedge thickness.

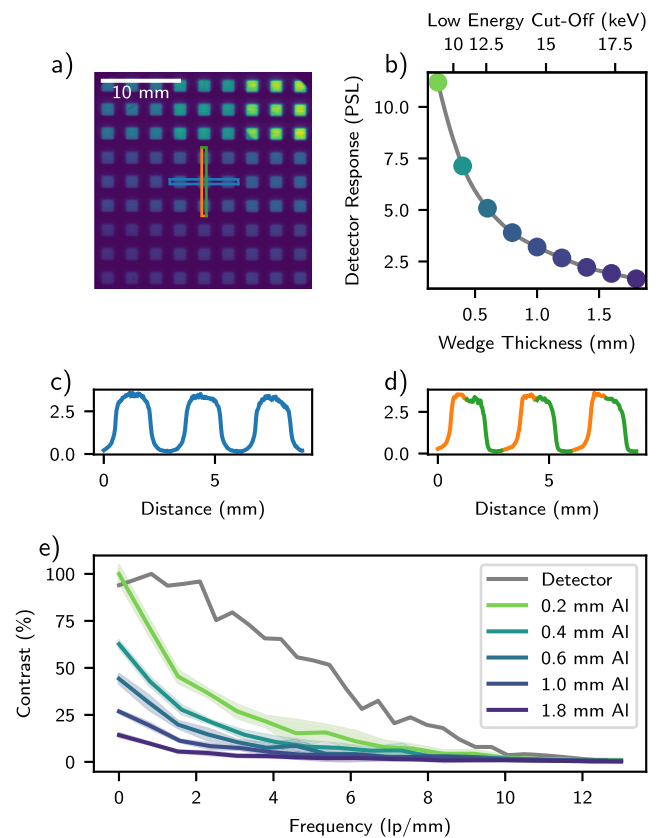


FIG. 5. Image plate data of the combined step-wedge and grid calibration target (a). The detector response is plotted against wedge thickness in (b), which was used to calibrate the flyer plate radiographs. Horizontal (c) and vertical (d) lineouts from the image plate data [indicated by the blue, orange, and green boxes in (a)] show asymmetries in the edge profiles. The modulation transfer function showing the contrast transferred by the imaging system over a range of resolutions for different wedge thicknesses is plotted in (e).

The step wedge was backed by a regular $1.5 \times 1.5 \text{ mm}^2$ grid cut from a $100 \mu\text{m}$ thick tungsten foil. It was positioned to have the same magnification as the imaging line so that the width of the grid edges is equal to the resolution of the image. Positioning the grid on the same line as the step wedge not only saves the number of diagnostic lines required to characterize the source but also means that the resolution in different spectral bands can be evaluated. Using a 2D grid also allows the resolution to be evaluated in both axes (horizontal and vertical), which is not necessarily equal for a structured X-pinch source.

The resolution was not found to be energy-dependent over the spectral range transmitted by the step wedge; however, Fig. 5(d) does show asymmetries in the vertical direction due to a structure in the source. The average resolutions in the horizontal and vertical directions are $490(50)$ and $400(70) \mu\text{m}$, respectively, which correspond to effective source sizes of $2.1(2)$ and $1.7(3) \text{ mm}$ using Eqs. (2) and (3). The discrepancy in the source size measured from the grid edges and pinhole camera is a result of the distributed source, with low intensity radiation contributing to the effective source size outside the region identified in the pinhole images.

Figure 5(e) shows the modulation transfer function (MTF) in the horizontal direction for a subset of grid thicknesses, displaying the contrast transferred by the imaging system at different resolutions. The contrast through each filter thickness falls at a rate proportional to the maximum, indicating that despite a reduction in intensity, the resolution (as defined by edge width) remains constant over the range of energies transmitted by the target. The MTF of the sharp edge used to calculate δ_{ip} in Sec. II was scaled to a 100% contrast and plotted on the same axis. This line represents the performance of the system in the absence of contributions from the source size, highlighting the potential for significant improvement in the image resolution by reducing the source size.

Filtered Si diodes were used to make time resolved measurements of x-ray flux in different spectral bands. This allowed the image plate data to be synchronized with the flyer plate dynamics and measurements of the hard x-ray pulse duration of 15 ns (FWHM). Future improvements in this diagnostic will allow time-resolved broadband measurements of the spectrum.

IV. RESULTS

The current and velocity data shown in Fig. 6 illustrate the overall dynamics of the flyer plate launch and the repeatability of the platform. Peak machine current was measured at 2 MA rising in $1.4 \mu\text{s}$ (dashed lines). The flyer plate accelerates to 4.2 km s^{-1} as measured with PDV (solid lines). Dry Pinch I was triggered independently of CEPAGE at 2.3 and $2.9 \mu\text{s}$ (dotted lines), while the flyer is still traversing the electrode recess. The flyer impacts the sample positioned at a flight distance of 9 mm at $3.9 \mu\text{s}$. Upon impact, the flyer drives a shock into the PMMA sample, which is sufficiently strong to attenuate or deflect the optical backlighter, such that the shock appears opaque, as shown in Fig. 6(b). The sample shock velocity is tracked and plotted in the dots shown in Fig. 6(a); it rapidly decayed from over 6 to 3 km s^{-1} as it crossed the 9 mm field of view. The flyer and shock velocities had average standard deviations of 1% and 2.5% over their trajectories between experiments.

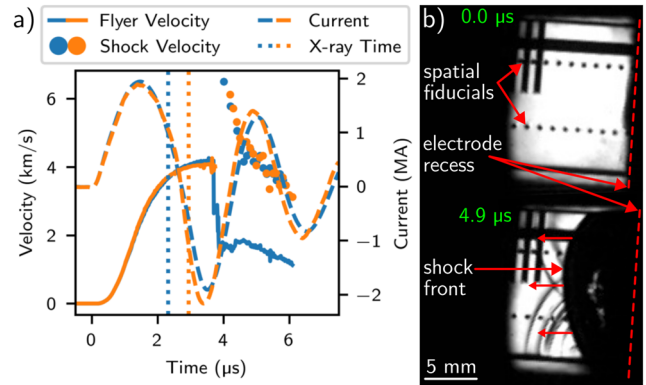


FIG. 6. Flyer velocity, sample shock velocity, machine current, and radiograph timing from two separate flyer plate experiments (a) and two example frames of the optical imaging line from the blue dataset (b). The shock velocities represented by the dots in (a) were calculated by temporally differentiating the position of the shock front measured across multiple backlight optical imaging frames, such as those in (b). The shock is propagating horizontally in (b); however, the PMMA sample is at a 3° angle to prevent back reflections when viewed along the PDV line of sight.

Figure 7 shows point projection radiographs of flyer plates produced with the X-pinch source. One static pre-shot image and two mid-flight images were captured (on separate experiments). The static image was taken without firing CEPAGE, while the two dynamic radiographs were timed to capture the flyer at different stages of launch. The image plate signal was converted to apparent areal density via the step wedge thickness using the calibration target, and the spatial scales were calculated from magnification. Note that these color maps do not necessarily represent the areal density because we have not accounted for changes in opacity due to the non-STP structure in the flyer. Despite this, these images enable us to identify features that are otherwise unobservable.

The bright yellow region is the vacuum gap between the anode and cathode. The purple region to the left is the electrode recess into which the flyer is accelerated during an experiment. The apparent areal density is unexpectedly high through the A-K gap and

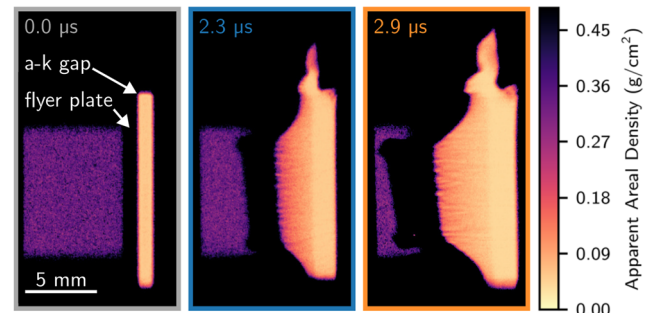


FIG. 7. Radiographs of the flyer plate. The flyer plate and A-K gap are annotated on the static shot (gray border). The two frames with colored borders are dynamic shots and correspond with the colored velocimetry data shown in Fig. 6(a).

recess walls, which should be 0 and 0.27 g cm^{-2} , respectively. This is attributed to 4 mm of additional polycarbonate shielding, which was in the radiography line of sight but was not accounted for in the calibration target line and contributes an additional 20% absorption for 20 keV x rays.

The dynamic radiography images capture the projection across the leading edge and structure behind the flyer plate. Flyer shape, tilt, and position in the recess can be measured from the leading edge and benchmarked against simulations. The flyer tilt is expected due to magnetic field enhancement at the connection between the electrodes. The flyer position in the recess is consistent with the integrated velocity time series from PDV to within the image resolution. The A–K gap extends vertically as the anode and the cathode are forced apart during the experiment. The density profile behind the flyer indicates the presence of a trailing mass. In cylindrical wire array implosions, the trailing mass is understood to provide a low inductance current path that hinders the stagnation of the Z pinch.^{21–23} In planar flyer plate geometry, it could limit the acceleration of the flyer. The periodic structure in the trailing mass behind the flyer is indicative of instability in growth. For a thinner flyer plate or a longer drive duration, this could result in the development of a magneto Rayleigh–Taylor (MRT) instability, which disrupts the front surface of the flyer plate. Consequently, this platform allows for the study of MRT instabilities in a well-diagnosed quasi-1D geometry.

V. CONCLUSION

A portable X-pinch driver was coupled to the CEPAGE generator and used capture point projection radiographs of dynamic flyer plate experiments. Two flyer plates were imaged at different times during their trajectory with a horizontal resolution of $490(50) \mu\text{m}$, providing new data on the 2D structure of the flyer plate, which can be used to benchmark in-house MHD simulations using B2. These frames reveal the structure behind the flyer, which is not observable with the conventional current and velocimetry diagnostics and to our knowledge, has not been previously studied.

Future work will aim to improve the resolution of the imaging system by testing different X-pinch loads to reduce the source size. In the longer term, detailed on-shot spectral measurements, combined with more advanced synthetic radiography software, can extend beyond the assumption of cold material opacities. This advancement will improve the accuracy of areal density calculations, enabling quantitative comparison to simulations. There is scope to extend this work to FLF's higher energy pulsed power driver, M3. On M3, the velocimetry signal is lost well before impact so 2D measurements of the front surface position will be instrumental in constraining the flyer velocity profile.

ACKNOWLEDGMENTS

The author would like to thank Jergus Strucka and Simon Bland of Imperial College, London, for the loan of their PDV system and their advice and support on operating Dry Pinch I.

AUTHOR DECLARATIONS

Conflict of Interest

The authors have no conflicts to disclose.

Author Contributions

J. Read: Conceptualization (equal); Formal analysis (equal); Investigation (equal); Methodology (equal); Project administration (equal); Writing – original draft (equal). **G. Burdiak:** Conceptualization (equal); Supervision (equal); Writing – review & editing (equal). **S. N. Bland:** Methodology (supporting); Resources (supporting); Writing – review & editing (supporting). **L. S. Caballero Bendixsen:** Formal analysis (supporting); Investigation (supporting); Writing – review & editing (supporting). **L. Paxton-Fear:** Formal analysis (supporting); Methodology (equal). **N. Niasse:** Conceptualization (supporting); Software (lead). **C. Dobranszki:** Investigation (supporting); Methodology (supporting). **N. Hawker:** Funding acquisition (lead).

DATA AVAILABILITY

The data that support the findings of this study are available from the corresponding author upon reasonable request.

REFERENCES

- 1 D. Sinars, M. Sweeney, C. Alexander, D. Ampleford, T. Ao, J. Apruzese, C. Aragon, D. Armstrong, K. Austin, T. Awe *et al.*, “Review of pulsed power-driven high energy density physics research on Z at Sandia,” *Phys. Plasmas* **27**, 070501 (2020).
- 2 D. B. Reisman, B. S. Stoltzfus, W. A. Stygar, K. N. Austin, E. M. Waisman, R. J. Hickman, J.-P. Davis, T. A. Haill, M. D. Knudson, C. T. Seagle, J. L. Brown, D. A. Goetz, R. B. Spielman, J. A. Goldlust, and W. R. Cravey, “Pulsed power accelerator for material physics experiments,” *Phys. Rev. Accel. Beams* **18**, 090401 (2015).
- 3 M. D. Knudson, M. P. Desjarlais, and A. Pribram-Jones, “Adiabatic release measurements in aluminum between 400 and 1200 GPa: Characterization of aluminum as a shock standard in the multimegabar regime,” *Phys. Rev. B* **91**, 224105 (2015).
- 4 J. Skidmore *et al.*, “A shock amplification platform for high-energy-density physics studies: Accessing terapascal pressures on a two-stage light-gas gun,” *Phys. Rev. Lett.* (Submitted) (2024).
- 5 S. V. Lebedev, F. N. Beg, S. N. Bland, J. P. Chittenden, A. E. Dangor, M. G. Haines, M. Zakoullah, S. A. Pikuz, T. A. Shelkovenko, and D. A. Hammer, “X-ray backlighting of wire array Z-pinch implosions using X pinch,” *Rev. Sci. Instrum.* **72**, 671–673 (2001).
- 6 T. A. Shelkovenko, D. B. Sinars, S. A. Pikuz, K. M. Chandler, and D. A. Hammer, “Point-projection x-ray radiography using an X pinch as the radiation source,” *Rev. Sci. Instrum.* **72**, 667–670 (2001).
- 7 T. A. Shelkovenko, S. A. Pikuz, and D. A. Hammer, “A review of projection radiography of plasma and biological objects in X-Pinch radiation,” *Plasma Phys. Rep.* **42**, 226–268 (2016).
- 8 T. A. Shelkovenko, S. A. Pikuz, C. L. Hoyt, A. D. Cahill, L. Atoyian, D. A. Hammer, I. N. Tilikin, A. R. Mingaleev, V. M. Romanova, and A. V. Agafonov, “A source of hard X-ray radiation based on hybrid X pinches,” *Phys. Plasmas* **23**, 103303 (2016).
- 9 S. V. Lebedev, F. N. Beg, S. N. Bland, J. P. Chittenden, A. E. Dangor, M. G. Haines, K. H. Kwek, S. A. Pikuz, and T. A. Shelkovenko, “Effect of discrete wires

- on the implosion dynamics of wire array Z pinches," *Phys. Plasmas* **8**, 3734–3747 (2001).
- ¹⁰J. D. Douglass, D. A. Hammer, S. A. Pikuz, T. A. Shelkovenko, and K. S. Blesener, "Plasma density measurements in tungsten wire-array Z-pinches," *Phys. Plasmas* **19**, 072710 (2012).
- ¹¹S. C. Bott, D. M. Haas, Y. Eshaq, U. Ueda, S. V. Lebedev, J. P. Chittenden, J. B. A. Palmer, S. N. Bland, G. N. Hall, D. J. Ampleford, and F. N. Beg, "Quantitative measurements of wire ablation in tungsten X-pinches at 80 kA," *IEEE Trans. Plasma Sci.* **36**, 2759–2764 (2008).
- ¹²S. A. Pikuz, T. A. Shelkovenko, D. B. Sinars, J. B. Greenly, Y. S. Dimant, and D. A. Hammer, "Multiphase foamlake structure of exploding wire cores," *Phys. Rev. Lett.* **83**, 4313–4316 (1999).
- ¹³J. Strucka, J. W. D. Halliday, T. Gheorghiu, H. Horton, B. Krawczyk, P. Moloney, S. Parker, G. Rowland, N. Schwartz, S. Stanislaus, S. Theocharous, C. Wilson, Z. Zhao, T. A. Shelkovenko, S. A. Pikuz, and S. N. Bland, "A portable X-pinch design for x-ray diagnostics of warm dense matter," *Matter Radiat. Extremes* **7**, 016901 (2021).
- ¹⁴A. Lefrançois, P.-Y. Chanal, G. Le Blanc, J. Petit, G. Avriilaud, and M. Delchambre, "High-velocity flyer-plate developments on two high-pulsed-power generators based on a strip-line design (GEPI and CEPAGE)," *IEEE Trans. Plasma Sci.* **39**, 288–293 (2011).
- ¹⁵T. Ao, J. R. Asay, S. Chantrenne, M. R. Baer, and C. A. Hall, "A compact strip-line pulsed power generator for isentropic compression experiments," *Rev. Sci. Instrum.* **79**, 013903 (2008).
- ¹⁶S. N. Bland, Y. E. Krasik, D. Yanuka, R. Gardner, J. MacDonald, A. Virozub, S. Efimov, S. Gleizer, and N. Chaturvedi, "Generation of highly symmetric, cylindrically convergent shockwaves in water," *Phys. Plasmas* **24**, 082702 (2017).
- ¹⁷R. W. Lemke, M. D. Knudson, and J.-P. Davis, "Magnetically driven hypervelocity launch capability at the Sandia Z accelerator," *Int. J. Impact Eng.* **38**, 480–485 (2011), part of Special Issue: Hypervelocity Impact Selected Papers from the 2010 Symposium.
- ¹⁸P. J. Turchi, M. L. Alme, G. Bird, C. N. Boyer, S. K. Coffey, D. Conte, J. F. Davis, and S. W. Seiler, "Review of plasma flow switch development," *IEEE Trans. Plasma Sci.* **15**, 747–759 (1987).
- ¹⁹B. Henke, E. Gullikson, and J. Davis, "X-ray interactions: Photoabsorption, scattering, transmission, and reflection at $E = 50$ -30,000 eV, $Z = 1$ -92," *At. Data Nucl. Data Tables* **54**, 181–342 (1993).
- ²⁰A. L. Meadowcroft, C. D. Bentley, and E. N. Stott, "Evaluation of the sensitivity and fading characteristics of an image plate system for x-ray diagnostics," *Rev. Sci. Instrum.* **79**, 113102 (2008).
- ²¹S. V. Lebedev, F. N. Beg, S. N. Bland, J. P. Chittenden, A. E. Dangor, and M. G. Haines, "Snowplow-like behavior in the implosion phase of wire array Z pinches," *Phys. Plasmas* **9**, 2293–2301 (2002).
- ²²M. E. Cuneo, E. M. Waisman, S. V. Lebedev, J. P. Chittenden, W. A. Stygar, G. A. Chandler, R. A. Vesey, E. P. Yu, T. J. Nash, D. E. Bliss, G. S. Sarkisov, T. C. Wagoner, G. R. Bennett, D. B. Sinars, J. L. Porter, W. W. Simpson, L. E. Ruggles, D. F. Wenger, C. J. Garasi, B. V. Oliver, R. A. Aragon, W. E. Fowler, M. C. Hettrick, G. C. Idzorek, D. Johnson, K. Keller, S. E. Lazier, J. S. McGurn, T. A. Mehlhorn, T. Moore, D. S. Nielsen, J. Pyle, S. Speas, K. W. Struve, and J. A. Torres, "Characteristics and scaling of tungsten-wire-array z-pinch implosion dynamics at 20 MA," *Phys. Rev. E* **71**, 046406 (2005).
- ²³G. C. Burdiak, S. V. Lebedev, G. N. Hall, A. J. Harvey-Thompson, F. Suzuki-Vidal, G. F. Swadling, E. Khoory, L. Pickworth, S. N. Bland, P. de Grouchy, and J. Skidmore, "Determination of the inductance of imploding wire array Z-pinches using measurements of load voltage," *Phys. Plasmas* **20**, 032705 (2013).